Date of publication xxxx 00, 0000, date of current version xxxx 00, 0000.

Digital Object Identifier 00.0000/ACCESS.2019.DOI

An ASAPPP Approach to the Spectrum Allocation in General Heterogeneous Cellular Networks

HAICHAO WEI[1], NA DENG[2,3], (Member, IEEE), and MARTIN HAENGGI[4], (Fellow, IEEE)

[1]School of Information Science Technology, Dalian Maritime University, Dalian, Liaoning, 116026, China (e-mail: weihaichao@dlmu.edu.cn)
[2]School of Information and Communication Engineering, Dalian University of Technology, Dalian, 116024, China
[3]National Mobile Communications Research Laboratory, Southeast University, Nanjing 210096, China
[4]Dept. of Electrical Engineering, University of Notre Dame, Notre Dame 46556, USA (e-mail: mhaenggi@nd.edu)

Corresponding author: Na Deng (e-mail: dengna@dlut.edu.cn).

This work was supported by the National Natural Science Foundation of China under Grant 61701071, by the China Postdoctoral Science Foundation (2017M621129), by the open research fund of National Mobile Communications Research Laboratory, Southeast University (No. 2019D03), by the Fundamental Research Funds for the Central Universities under Grants DUT19RC(4)014 and 3132019220, and by the US NSF grant CCF 1525904.

ABSTRACT The increasing heterogeneity of cellular networks makes the signal-to-interference-ratio (SIR) distribution challenging to derive, which restricts the further analysis of metrics that depend on it. In this paper, we establish a general heterogeneous cellular network (HCN) model to investigate the problem of spectrum allocation to the different tiers and propose an equivalent orthogonal network (EON) model to formulate the optimization problems. Specifically, we first employ the ASAPPP method which refers to "an approximate SIR analysis based on the Poisson point process" to provide accurate approximations to the spectral and energy efficiency in the EON. The approximations are then applied to spectrum allocation optimization problems, where the optimal SIR thresholds are derived, and, in turn, the optimal solutions are obtained that maximize the area spectral efficiency (ASE) and network energy efficiency (NEE), respectively. Interestingly, the optimal SIR threshold can be well approximated by an extremely simple expression that merely depends on the path loss exponent alone. The results indicate that neither full spectrum sharing nor full spectrum partitioning are optimal for all network parameters, such as density, transmit power, etc., in terms of both the ASE and NEE. Instead, a hybrid scheme may perform the best. Moreover, different constraints on the spectrum efficiency can have a drastic impact on the performance of spectrum allocation schemes.

INDEX TERMS Heterogeneous cellular networks, ASAPPP, Spectrum allocation, Poisson point process, Stochastic geometry.

I. INTRODUCTION

A. MOTIVATION

Heterogeneous cellular networks (HCNs) have gained much momentum in the wireless industry and research communities. In the context of HCNs, spectrum allocation plays an important role in both user-perceived and network-level performances due to the tradeoff associated with spectrum sharing and partitioning [1]. Spectrum sharing increases the bandwidth efficiency at the expense of high inter-tier interference, while spectrum partitioning eliminates the inter-tier interference at the cost of lower spectrum utilization. Since future networks are fusions of multi-standard and multi-band networks, some types of wireless access points (with different radio technologies) operate in non-overlapping frequency bands while other types of wireless radio points share the same spectrum band. It means that spectrum sharing and partitioning schemes are likely to coexist in the future networks. This complicated network configuration greatly exacerbates the spectrum allocation problem in HCNs. Hence, for general HCNs, it is crucial to explore efficient techniques for tractable analysis and find the optimal operating regime of the spectrum allocation.

B. RELATED WORK

One line of works concerning the spectrum allocation issues focuses on finite network scenarios with different

objective functions and constraints [2–6], where the scenarios with hexagonally deployed macro cells or one macro cell overlaid by small cells are considered. However, the increasing heterogeneity and density in cellular networks renders the traditional hexagonal models of limited utility and motivates another line of studies based on stochastic geometry, where various point process models accurately capture different spatial characteristics of network nodes. Given the need for interference characterization, stochastic geometry has emerged as a powerful mathematical tool to simplify the modeling and quantify the fundamental performance of wireless networks in different research fields [7–15]. Most of the stochastic geometry works on HCNs assume that base station (BS) deployments of different types follows mutually independent Poisson point processes (PPP) [9, 10] to investigate the user-perceived performance (e.g., signal-to-interference-ratio (SIR) distribution or transmission rate) in [11, 12] and network-level performance (e.g., throughput, area spectral efficiency (ASE) or network utility) in [13–15]. Although this common assumption makes the analysis tractable, it does not capture the spatial correlation between BSs. For instance, the macro BSs usually exhibit spatial repulsion [16] while the small cells covering the hotspots exhibit clustering [17]. Therefore, non-Poisson network models should be adopted to capture these actual spatial characteristics and investigate the spectrum allocation issues in general HCNs. However, for the non-Poisson models suitable for real deployments [16–18] such as the perturbed lattice, the β-Ginibre point process (β-GPP), clustering point process, etc., it is difficult (or even impossible) to derive exact results for the SIR distributions and the further metrics strongly depending on the SIR distribution in single-tier network, let alone in HCNs. As a consequence, a further analysis and comparison of spectrum allocation schemes are prohibitively complicated.

Fortunately, the ASAPPP (approximate SIR analysis based on the PPP) method [19] for single-tier networks yields a simple yet accurate approximation of the SIR distribution for general cellular networks modeled as non-Poisson deployments [20, 21], and our previous work [22] extends the approximative analysis of the SIR distributions to general HCNs. Based on the ASAPPP method, a very recent work [23] provides a fine-grained analysis of the SIR in both single-tier and multi-tier general cellular networks using the concept of the SIR meta distribution introduced in [24]. Due to its simplicity, the ASAPPP method permits a further analysis and optimization of other performance metrics, including the analysis and design of spectrum allocation schemes for all stationary network models. In this work, we will fill this gap with new analytical results on the key network-level performance metrics of both ASE and network energy efficiency (NEE). As ASAPPP captures all stationary deployments [21], it reflects the characteristics of realistic cellular systems including LTE deployments as well as 5G deployments, and the corresponding analytical results can provide key guidelines for system design and planning.

C. CONTRIBUTIONS

In this paper, we propose a novel framework to investigate spectrum allocation schemes for general HCNs based on the approximative SIR distribution obtained by the ASAPPP method. The specific contributions are summarized as follows.

- We propose an equivalent orthogonal network model to capture the coexistence of spectrum sharing and partitioning among different tiers in general HCNs. For two key performance metrics (ASE and NEE), we formulate the corresponding spectrum allocation optimization problem under different spectral efficiency (SE) constraints for users of each tier. The maximization problem is solved by decomposing it into two subproblems that can be solved consecutively.
- The first subproblem is to obtain the optimal SIR thresholds corresponding to the maximal spectral efficiency through the ASAPPP method. We provide an extremely simple approximation to the optimal SIR threshold that merely depends on the path loss exponent alone, based on which a simple yet accurate approximation is obtained for the maximal spectral efficiency. Then the second subproblem gives the optimal spectrum allocation based on the solution of the first one.
- For full spectrum sharing and full spectrum partitioning as well as hybrid cases, the results show that these three cases have their own optimum operating regimes in terms of both the ASE and NEE with different system parameters, such as the density, transmit power, etc.
- Different constraints for the spectrum efficiency significantly affect the performance of each spectrum allocation case and change the optimal spectrum allocation schemes.

II. SYSTEM MODEL

A. NETWORK MODEL

We consider a general K-tier heterogeneous network in the interference-limited regime where the locations of the BSs in the k-th tier are modeled as an independent stationary point process Φ_k, $k \in [K]$ with $[K] \triangleq \{1, 2, \ldots, K\}$. Let μ_k and λ_k be the transmit power and node density of tier k, respectively. We suppose that the total bandwidth is split into $M \leq K$ parts, where the m-th part, $m \in [M]$, is allocated the fractional bandwidth b_m and shared by tiers in the subset $\mathcal{T}_m \subseteq [K]$. We assume $\mathcal{T}_i \cap \mathcal{T}_j = \emptyset$ for $i \neq j$, i.e., there are no common tiers in different $\mathcal{T}_m$. In other words, $\mathcal{T}_m, m \in [M]$, is a partition of the tier set $[K]$. The number of possible partitions is the K-th Bell number. Specifically, $M = 1$ means full spectrum sharing, $M = K$ means full spectrum partitioning, and $1 < M < K$ refers to hybrid schemes of both spectrum sharing and partitioning for different bands in the networks. It is assumed that all the BSs are fully loaded, which is a common assumption when evaluating the network performance at peak load. Each user is associated with the BS that offers the strongest average received power, and each

BS is assumed to serve its associated users in a time-division fashion.

We further assume a power path loss law $\ell(x) = |x|^{-\alpha}$ with a path loss exponent α and independent Rayleigh fading with unit mean, $\mathbb{E}(h) = 1$. Due to the stationarity of all Φ_k, we consider the typical k-th tier user located at the origin and the received SIR for the k-th type user is expressed as

$$\mathrm{SIR}_k \triangleq \frac{S_k}{I_k} = \frac{\mu_k \ell(x_0) h_{x_0}}{\sum_{i\in\mathcal{T}_{\nu(k)}} \sum_{x\in\Phi_i\setminus\{x_0\}} \mu_i \ell(x) h_x}, \quad (1)$$

where x_0 denotes the location of the serving BS in tier k, $\nu(k)$ returns the index of the bandwidth part used by tier k, and h_x is the power fading coefficient associated with x. For an arbitrary user, the coverage probability is defined as

$$P_{\mathrm{c}}(\theta) \triangleq \sum_{k\in[K]} \mathbb{P}(\mathrm{SIR}_k > \theta, x_0 \in \Phi_k), \quad (2)$$

where θ is the target SIR threshold. In other words, the coverage probability is the complementary cumulative distribution (ccdf) $\bar{F}_{\mathrm{SIR}}(\theta)$ of the received SIR, i.e., $P_{\mathrm{c}}(\theta) \equiv \bar{F}_{\mathrm{SIR}}(\theta)$. To facilitate the following analysis, we also define the coverage probability of the users served by tier k as $P_k(\theta) \triangleq \mathbb{P}(\mathrm{SIR}_k > \theta)$.

B. THE EQUIVALENT ORTHOGONAL NETWORK MODEL

According to the spectrum allocation to the different tiers, the original K-tier general HCN can be logically restructured into a HCN with M composite tiers, where the m-th composite tier is allocated the fractional bandwidth b_m. Hence, no inter-composite-tier interference occurs, and M composite tiers constitute an *equivalent orthogonal network*, which is defined as follows.

Definition 1 (**Equivalent Orthogonal Network, EON**). *Let $\Phi_k, k \in [K]$ be a point process modeling the locations of the k-tier BSs with density λ_k, and $b_m, m \in [M]$, be the m-th fractional bandwidth of the available spectrum. Denote by $\mathcal{T}_m, m \in [M]$, a partition of the tier set $[K]$. The equivalent orthogonal network model is defined as*

$$\tilde{\Phi}_m \triangleq \bigcup_{k\in\mathcal{T}_m} \Phi_k, \quad m \in [M], \quad (3)$$

where composite tier $\tilde{\Phi}_m$ uses the m-th fractional bandwidth and its density is $\tilde{\lambda}_m = \Sigma_{k\in\mathcal{T}_m} \lambda_k$.

Through the EON model, general spectrum allocation schemes (full spectrum sharing, full spectrum partitioning, and hybrid schemes) can be converted into the spectrum partitioning between different composite tiers, which significantly simplifies the performance analysis.

III. THE ASAPPP APPROACH

Since the coverage probability is a fundamental metric for further analysis, we give a tractable and accurate approximation based on the ASAPPP method. Specifically, the coverage probability for the tiers with dedicated spectrum is approximated by standard ASAPPP (termed *single-tier ASAPPP*) method [20, 21], and the one with shared spectrum is approximated by the effective gain ASAPPP (termed *multi-tier ASAPPP*) method [22].

1) Single-tier ASAPPP

The most tractable model for the BS locations is the homogeneous PPP model [20], and the ccdf of the SIR with Rayleigh fading is given as [21]

$$\bar{F}^{\mathrm{PPP}}_{\mathrm{SIR}}(\theta) = \frac{1}{{}_2F_1(1, -\delta, 1-\delta, -\theta)}, \quad (4)$$

where $\delta = 2/\alpha$ and ${}_2F_1$ is the Gaussian hypergeometric function [25, Eqn. 15.3.1]. Since the locations of the BSs in each tier follow a general stationary point process, it is difficult (most likely impossible) to directly obtain an exact analytical expression of the coverage probability, which imposes restrictions on the further analysis for other key performance metrics based on the SIR. Hence it is of great importance to investigate good and universal approximation techniques to characterize the performance metrics for general network models.

It has recently been shown in [21] that the SIR distribution of single-tier non-Poisson networks can be accurately approximated by that of a Poisson network through scaling the threshold θ with a certain factor G, i.e.,

$$\bar{F}_{\mathrm{SIR}}(\theta) \approx \bar{F}^{\mathrm{PPP}}_{\mathrm{SIR}}(\theta/G). \quad (5)$$

This approach of approximating the SIR distribution is called ASAPPP method [19], which stands for "approximate SIR analysis based on the PPP" and can also be read as "as a PPP", indicating that the network is first treated as if it forms a PPP and then a shift (in dB) is applied to the SIR distribution. This shift can be regarded as the *SIR gain* of the non-Poisson model over the Poisson one, and it can be quantified using the mean interference-to-signal ratio (MISR) as

$$G = \frac{\mathrm{MISR}_{\mathrm{PPP}}}{\mathrm{MISR}}. \quad (6)$$

The MSIR is defined as [20]

$$\mathrm{MISR} \triangleq \mathbb{E}\left\{\frac{I}{\mathbb{E}_h(S)}\right\} = \mathbb{E}\left\{\frac{\sum_{x\in\Phi\setminus\{x_0\}} \ell(x)}{\ell(x_0)}\right\} \quad (7)$$

for a network with base stations located at Φ with serving BS x_0. $\mathbb{E}_h(S) = \mu_{x_0}\ell(x_0)$ is the signal power averaged over the fading. Hence the MISR is a purely geometric quantity that is independent of the fading model. The MISR for Poisson networks can be analytically derived as $\mathrm{MISR}_{\mathrm{PPP}} = 2/(\alpha-2)$ [20]. For other stationary point processes, the analytical expressions of the MISR and the asymptotic gain are currently unavailable, and thus one resorts to simulation approaches or the approximate expression in [26]. For repulsive point processes, $G > 1$, while for clustered point processes, $G < 1$.

As shown in [21], the approximation is asymptotically exact as $\theta \to 0$, i.e.,

$$\bar{F}_{\mathrm{SIR}}(\theta) \sim \bar{F}^{\mathrm{PPP}}_{\mathrm{SIR}}(\theta/G), \quad \theta \to 0, \quad (8)$$

and thus the SIR gain is also termed the asymptotic gain. Furthermore, the error of the approximation based on the asymptotic gain is tightly bounded over the entire range of θ, and robust for different path loss exponents and fading models [21]. The single-tier ASAPPP is used to approximate the coverage probability for the tiers with dedicated spectrum allocation, i.e., no inter-tier interference, and we have

$$P_k(\theta) \approx \bar{F}_{\mathrm{SIR}}^{\mathrm{PPP}}(\theta/G_k), \quad \text{for } \#\mathcal{T}_{\nu(k)} = 1, \tag{9}$$

where $P_k(\theta)$ is the coverage probability of users in tier k, G_k is the corresponding SIR gain, and $\#\mathcal{A}$ denotes the cardinality of the set $\mathcal{A}$.

2) Multi-tier ASAPPP

The above results are only valid in the case without inter-tier interference. If the m-th part of the bandwidth is shared by multiple tiers in $\mathcal{T}_m$, i.e., $\#\mathcal{T}_m > 1$, single-tier ASAPPP can not directly yield the approximative coverage probability. Hence we apply the effective gain ASAPPP method for HCNs [22] to approximate the coverage probability by scaling the threshold θ with the effective SIR gain, which is determined by relative transmit powers and densities and the SIR gains of tiers sharing the spectrum resource.

Through the ASAPPP methods for single-tier and multi-tier networks, the following proposition provides an accurate approximation to the coverage probability of an arbitrary composite tier in the EON.

Proposition 1. *Let* $w_i \triangleq \frac{\lambda_i \mu_i^{\delta}}{\sum_{k\in\mathcal{T}_m} \lambda_k \mu_k^{\delta}}$ *and*

$$\tilde{G}_m \triangleq 1 + \sum_{i\in\mathcal{T}_m} w_i^2 (G_i - 1). \tag{10}$$

The coverage probability of the users served by composite tier m *in the EON is accurately approximated as*

$$P_m(\theta) \approx \bar{F}_{\mathrm{SIR}}^{\mathrm{PPP}}(\theta/\tilde{G}_m). \tag{11}$$

Proof: For a composite tier with $\mathcal{T}_m = \{k\}$ in the EON, the coverage probability is approximated via the single-tier ASAPPP method, given by

$$P_m(\theta) \approx \bar{F}_{\mathrm{SIR}}^{\mathrm{PPP}}(\theta/G_k), \tag{12}$$

and we also obtain $\tilde{G}_m = G_k$ per (10). For a composite tier with $\#\mathcal{T}_m > 1$ in the EON, the multi-tier ASAPPP method approximates the coverage probability with the effective gain per (10) and (11). ■

IV. AREA SPECTRAL EFFICIENCY OPTIMIZATION

A. PROBLEM FORMULATION FOR PER-TIER SPECTRUM ALLOCATION

Under a fixed-rate transmission, the area spectral efficiency of composite tier m is defined as [7]

$$\mathrm{ASE}_m \triangleq \tilde{\lambda}_m b_m P_m(\theta_m) \log_2(1+\theta_m), \tag{13}$$

where $c_m(\theta_m) = P_m(\theta_m)\log_2(1+\theta_m)$ is the achieved SE of the typical user served by the m-th composite tier. Summing over $[M]$, we obtain the overall area spectral efficiency of the HCN as

$$\mathrm{ASE}(\boldsymbol{\theta}, \boldsymbol{b}) = \sum_{m\in[M]} \tilde{\lambda}_m b_m P_m(\theta_m) \log_2(1+\theta_m), \tag{14}$$

where $\boldsymbol{b} = (b_1, b_2, \ldots, b_M)$ and $\boldsymbol{\theta} = (\theta_1, \theta_2, \ldots, \theta_M)$.

Here we consider an optimization problem termed *ASE Maximization with EON Spectrum Partitioning*. Specifically, given an EON model, the optimization problem is to maximize the ASE by jointly optimizing $\boldsymbol{b}$ and $\boldsymbol{\theta}$, where $\boldsymbol{b}$ presents the fraction of spectrum allocated to each composite tier and $\boldsymbol{\theta}$ parameterizes to the specific modulation and coding schemes used in each composite tier. The corresponding problem is formulated as

$$\begin{aligned} &\max_{\boldsymbol{b},\boldsymbol{\theta}} \mathrm{ASE}(\boldsymbol{\theta}, \boldsymbol{b}), \\ &\text{subject to} \sum_{m\in[M]} b_m = 1, \quad \boldsymbol{b}, \boldsymbol{\theta} \in (\mathbb{R}^+)^M. \end{aligned} \tag{15}$$

Let $\boldsymbol{\theta}^*$ be the vector of SIR thresholds that maximize $c_m(\theta_m)$, $m \in [M]$. Inspecting Problem (15), it can be seen that

$$\begin{aligned} \mathrm{ASE}(\boldsymbol{\theta}, \boldsymbol{b}) &= \sum_{m\in[M]} \tilde{\lambda}_m b_m c_m(\theta_m) \\ &\le \sum_{m\in[M]} \tilde{\lambda}_m b_m c_m(\theta_m^*) = \mathrm{ASE}(\boldsymbol{\theta}^*, \boldsymbol{b}), \quad \forall \boldsymbol{\theta}, \boldsymbol{b}. \end{aligned}$$

This shows that the maximization of $\mathrm{ASE}(\boldsymbol{\theta}, \boldsymbol{b})$ can be performed by maximizing $\mathrm{ASE}(\boldsymbol{\theta}^*, \boldsymbol{b})$ over $\boldsymbol{b}$, and the optimal SIR thresholds that maximize the overall ASE are the ones that maximize $c_m(\theta_m)$, $m \in [M]$. As a result, the optimization can be carried out in two steps, first over $\boldsymbol{\theta}$ and then $\boldsymbol{b}$, which implies that Problem (15) can be decomposed into the following two consecutive subproblems:

$$\begin{aligned} \text{Subproblem 1: } c_m^* &= \max_{\theta_m} P_m(\theta_m)\log_2(1+\theta_m) \\ &\approx \frac{1}{\ln 2} \max_{\theta_m} \frac{\ln(1+\theta_m)}{{}_2F_1(1, -\delta, 1-\delta, -\frac{\theta_m}{\tilde{G}_m})} \end{aligned} \tag{16}$$

$$\begin{aligned} \text{Subproblem 2: } &\max_{\boldsymbol{b}} \sum_{m\in[M]} \tilde{\lambda}_m b_m c_m^*, \\ &\text{subject to} \sum_{m\in[M]} b_m = 1, \quad \boldsymbol{b} \in (\mathbb{R}^+)^M \end{aligned} \tag{17}$$

B. SOLUTION OF SUBPROBLEMS

For Subproblem 1, each composite tier can be treated in isolation, and the goal is to find the optimal SIR threshold that maximizes the spectral efficiency $c_m(\theta_m)$. It is hard to obtain the maximum by taking the derivatives w.r.t. θ_m due to the complexity of the Gaussian hypergeometric function. Therefore, we first use the following lemma to reduce the feasible region of θ_m^* to a finite interval and then obtain the optimal solution using the **fminbnd** function in Matlab.

Lemma 1. *Letting $\mathcal{W}(x)$ be the Lambert $\mathcal{W}$ function which solves $\mathcal{W}(x)e^{\mathcal{W}(x)} = x$,*

$$z_m(\theta) \triangleq \frac{\ln(1+\theta)}{{}_2F_1(1,-\delta,1-\delta,-\theta/\tilde{G}_m)}, \tag{18}$$

$$\zeta_m \triangleq e^{\mathcal{W}\left(e^{1-\alpha}\left((\alpha/2-1)\tilde{G}_m+1-\alpha\right)\right)+\alpha-1} - 1, \tag{19}$$

the global maximum of $z_m(\theta)$ is achieved in $(0, \zeta_m)$.

Proof: The derivative of $z_m(\theta)$ can be written as $z'_m(\theta) = \kappa(\theta)s(\theta)$, where $\kappa(\theta) > 0$ for all $\theta > 0$ and $s(\theta)$ is given by

$$\begin{aligned} s(\theta) = {} & \tilde{G}_m(1-\delta){}_2F_1(1,-\delta,1-\delta,-\theta/\tilde{G}_m) \\ & -\delta(1+\theta)\ln(1+\theta){}_2F_1(2,1-\delta,2-\delta,-\theta/\tilde{G}_m). \end{aligned} \tag{20}$$

Since the monotonicity of $z_m(\theta)$ depends on the sign of its first derivative, whose sign is the same as that of the above expression, we have $\text{sign}(z'_m(\theta)) = \text{sign}(s(\theta))$ for all $\theta > 0$. Due to the hypergeometric differential equation [25, Eqn. 15.5.1] and differentiation formula [25, Eqn. 15.2.2], we obtain

$$\begin{aligned} & {}_2F_1\left(1,-\delta,1-\delta,-\theta/\tilde{G}_m\right) \\ & = {}_2F_1\left(3,2-\delta,3-\delta,-\frac{\theta}{\tilde{G}_m}\right)\frac{2\theta(\tilde{G}_m+\theta)}{\tilde{G}_m^2(\delta-2)} \\ & + \frac{(1-\delta)\tilde{G}_m+(2-\delta)\theta}{(1-\delta)\tilde{G}_m}{}_2F_1(2,1-\delta,2-\delta,-\theta/\tilde{G}_m). \end{aligned} \tag{21}$$

Letting

$$\eta_m(\theta) = (1-\delta)\tilde{G}_m + (2-\delta)\theta - \delta(1+\theta)\ln(1+\theta), \tag{22}$$

we have

$$\begin{aligned} s(\theta) = {} & \frac{-2\theta(\tilde{G}_m+\theta)(1-\delta)}{\tilde{G}_m(2-\delta)}{}_2F_1(3,2-\delta,3-\delta,-\theta/\tilde{G}_m) \\ & + {}_2F_1(2,1-\delta,2-\delta,-\theta/\tilde{G}_m)\eta_m(\theta). \end{aligned} \tag{23}$$

From the integral representation [25, Eqn. 15.3.1], both Gaussian hypergeometric functions in (23) are greater than 0 when $\theta \geq 0$. Therefore, when $\eta_m(\theta) \leq 0$, we have $s(\theta) < 0$. We can easily prove that the equation $\eta_m(\zeta_m) = 0$ has a unique root ζ_m in $[0, \infty)$ and when $\theta \geq \zeta_m$, we have $\eta_m(\theta) < 0$ and $s(\theta) < 0$. It means that $z_m(\theta)$ is a decreasing function for $\theta \in [\zeta_m, \infty]$.

Consequently, the global maximum of $z_m(\theta)$ is achieved in $(0, \zeta_m)$. After a few steps, we find that the root of $\eta_m(\zeta_m)$ is given by

$$e^{\rho_m}\rho_m = e^{1-\alpha}\left((\alpha/2-1)\tilde{G}_m + 1 - \alpha\right) \tag{24}$$

where $\rho_m = \ln(1+\zeta_m) + 1 - \alpha$. Therefore, we obtain (19) using the Lambert $\mathcal{W}$ function. ∎

Subproblem 2 is an easily-solved linear program based on the optimal solution of Subproblem 1. In order to maximize the overall ASE, the optimal spectrum allocation is to allocate the total spectrum resource to the composite tier with the maximal $\tilde{\lambda}_m c^*_m$, i.e., to set

$$b_m = \mathbf{1}(m = \text{argmax}_{i\in[M]}\tilde{\lambda}_i c^*_i), \tag{25}$$

where $\mathbf{1}(\cdot)$ is the indicator function. Hence, if the goal is ASE maximization, the entire bandwidth is allocated to a single (composite) tier, i.e., the HCN logically degenerates to a single-tier network. This changes if we factor in other constraints, such as deployment cost, user distribution, and fairness. The result without extra constraints serves as a benchmark for comparison.

C. OPTIMIZATION WITH CONSTRAINTS

In the following, we consider two types of constraints appended to the optimization problem.

Firstly, we consider the minimum SE constraint to guarantee a minimum user performance in each tier. The minimum SE requirement for tier k is denoted by R_k. For Problem (15), this constraint is expressed as

$$b_m P_m(\theta_m)\log_2(1+\theta_m) \geq R_m, \tag{26}$$

where R_m is the minimum SE requirement of composite tier m and $R_m = \max_{k\in\mathcal{T}_m} R_k$. The revised problem can also be solved in two steps, first over $\boldsymbol{\theta}$ and then $\boldsymbol{b}$. Therefore, two similar subproblems can be obtained where the first one for $\boldsymbol{\theta}^*$ is the same as (16) and the second one is given with the introduction of the minimum SE constraints based on (17), given by

$$\begin{aligned} \text{Subproblem 2': } & \max_{\boldsymbol{b}} \sum_{m\in[M]} \tilde{\lambda}_m b_m c^*_m, \\ & \text{subject to } b_m c^*_m \geq R_m, \\ & \sum_{m\in[M]} b_m = 1, \quad \boldsymbol{b} \in (\mathbb{R}^+)^M. \end{aligned} \tag{27}$$

Accordingly, $\boldsymbol{\theta}^*$ is obtained as in Section IV-B. For the bandwidth allocation, we first assign the minimum bandwidth fraction $b^0_m = R_m/c^*_m$, $m \in [M]$, that satisfies the minimum SE constraint and then check whether $\sum_{m\in[M]} b^0_m \leq 1$ is satisfied. If satisfied, the remaining bandwidth is allocated to the tier with maximal $\tilde{\lambda}_m c^*_m$, i.e.,

$$b_m = 1 - \sum\nolimits_{j\in[M]\setminus\{m\}} b^0_j, \tag{28}$$

where $m = \text{argmax}_{i\in[M]}\tilde{\lambda}_i c^*_i$ and we obtain the maximal overall area spectral efficiency. If not, the revised problem has no solution.

Secondly, we consider the fairness constraint that users of each composite tier should achieve equal SE, expressed as

$$b_m P_m(\theta_m)\log_2(1+\theta_m) = c, \tag{29}$$

where c is the maximum common SE achievable. For each tier, we have $b_m c^*_m = c$, and with the sum constraint $\sum_{m\in[M]} b_m = 1$, we obtain

$$c = \frac{1}{\Sigma_{m\in[M]} 1/c^*_m}, \tag{30}$$

and $b_m = c/c_m^*$. Thus the sum spectral efficiency cM equals the harmonic mean of the individual spectral efficiencies c_m^*.

V. NETWORK ENERGY EFFICIENCY OPTIMIZATION

Since the energy consumption of cellular networks is dominated by the energy used at the BSs, we use a linear power consumption model as [27]

$$\xi_k = a_k \mu_k + \varpi_k, \quad k \in [K], \tag{31}$$

where a_k denotes the power amplifier efficiency at the transmit power μ_k and ϖ_k is the static power consumption (e.g., circuit power consumption, climate control, signal processing, etc.), independent of the transmit power. The network-level energy efficiency is defined as the ratio of the area spectrum efficiency to the area power consumption [27], expressed by

$$\mathrm{NEE}(\boldsymbol{b}, \boldsymbol{\theta}) = \frac{\sum_{m\in[M]} \tilde{\lambda}_m b_m P_m(\theta_m) \log_2(1+\theta_m)}{\sum_{m\in[M]} \sum_{k\in\mathcal{T}_m} \lambda_k \xi_k \mathbf{1}(b_m > 0)}. \tag{32}$$

Here we consider an optimization problem termed *NEE Maximization with EON Spectrum Partitioning*. Specifically, given an EON model, the optimization problem is to maximize the NEE by jointly optimizing $\boldsymbol{b}$ and $\boldsymbol{\theta}$, and the corresponding problem is formulated as

$$\begin{aligned} &\max_{\boldsymbol{b},\boldsymbol{\theta}} \mathrm{NEE}(\boldsymbol{b}, \boldsymbol{\theta}), \\ &\text{subject to } \sum\nolimits_{m\in[M]} b_m = 1, \quad \boldsymbol{b}, \boldsymbol{\theta} \in (\mathbb{R}^+)^M. \end{aligned} \tag{33}$$

Similar to the ASE optimization, it can also be seen that

$$\begin{aligned} \mathrm{NEE}(\boldsymbol{\theta}, \boldsymbol{b}) &= \frac{\sum\limits_{m\in[M]} \tilde{\lambda}_m b_m c_m(\theta_m)}{\sum\limits_{m\in[M]} \sum\limits_{k\in\mathcal{T}_m} \lambda_k \xi_k \mathbf{1}(b_m > 0)} \\ &\le \frac{\sum\limits_{m\in[M]} \tilde{\lambda}_m b_m c_m(\theta_m^*)}{\sum\limits_{m\in[M]} \sum\limits_{k\in\mathcal{T}_m} \lambda_k \xi_k \mathbf{1}(b_m > 0)} \\ &= \mathrm{NEE}(\boldsymbol{\theta}^*, \boldsymbol{b}), \quad \forall \boldsymbol{\theta}, \boldsymbol{b}. \end{aligned} \tag{34}$$

Therefore, the optimization can be also carried out in two consecutive steps, first over $\boldsymbol{\theta}$ and then $\boldsymbol{b}$, and Problem (33) can also be decomposed into two subproblems, where Subproblem 1 is the same as (16) and Subproblem 2 becomes

$$\begin{aligned} \text{Subproblem 2: } &\max_{\boldsymbol{b}} \frac{\sum\limits_{m\in[M]} \tilde{\lambda}_m b_m c_m^*}{\sum\limits_{m\in[M]} \sum\limits_{k\in\mathcal{T}_m} \lambda_k \xi_k \mathbf{1}(b_m > 0)}, \\ &\text{subject to} \sum_{m\in[M]} b_m = 1, \quad \boldsymbol{b} \in (\mathbb{R}^+)^M. \end{aligned} \tag{35}$$

Since the denominator of the objective function depends on the spectrum allocation variables $\boldsymbol{b}$, the solution of this Subproblem 2 can not be obtained as straightforwardly as for the ASE optimization. However, the following lemma shows that spectrum allocation problems in the NEE case have a similar property as in the ASE case.

Lemma 2. *The optimal solution of Subproblem 2 that maximizes the NEE is to merely allocate all the bandwidth to a certain composite tier.*

Proof: Firstly, we assume that the optimal solution is to allocate the spectrum resource to $n > 1$ composite tiers, say $l_1, \ldots, l_n$, and the maximum NEE is given by

$$\mathrm{NEE}^* = \frac{\sum\limits_{i=1}^{n} \tilde{\lambda}_{l_i} b_{l_i} c_{l_i}^*}{\sum\limits_{i=1}^{n} \sum\limits_{k\in\mathcal{T}_{l_i}} \lambda_k \xi_k}. \tag{36}$$

However, it is obvious to obtain

$$\mathrm{NEE}^* < \frac{\tilde{\lambda}_{l_m} c_{l_m}^*}{\sum\limits_{k\in\mathcal{T}_{l_m}} \lambda_k \xi_k}, \tag{37}$$

where $l_m = \mathrm{argmax}_{i\in\{l_1,\ldots,l_n\}} \tilde{\lambda}_i c_i^*$, and a contradiction occurs that there is another solution to achieve a larger NEE than the optimal one. Therefore, the initial assumption that the optimal solution is to allocate all the bandwidth to $n > 1$ composite tiers must be false, and the optimal solution allocates the entire spectrum resource to just one composite tier. ■

With the help of Lemma 2, the optimal spectrum allocation that maximizes the NEE is given by

$$b_m = \mathbf{1}\Big(m = \mathrm{argmax}_{i\in[M]} \frac{\tilde{\lambda}_i c_i^*}{\sum_{k\in\mathcal{T}_i} \lambda_k \xi_k}\Big). \tag{38}$$

Furthermore, we also consider the minimum and fairness SE constraints. Following the same reasoning in (34), the revised problem can also be solved in two steps, first over $\boldsymbol{\theta}$ and then $\boldsymbol{b}$. Therefore, two similar subproblems can be obtained where the first one for $\boldsymbol{\theta}^*$ is the same as (16) and the second one is given with the introduction of extra constraints based on (35). For the minimum SE constraints, Subproblem 2 becomes

$$\begin{aligned} \text{Subproblem 2': } &\max_{\boldsymbol{b}} \frac{\sum\limits_{m\in[M]} \tilde{\lambda}_m b_m c_m^*}{\sum\limits_{m\in[M]} \sum\limits_{k\in\mathcal{T}_m} \lambda_k \xi_k}, \\ &\text{subject to } b_m c_m^* \ge R_m, \\ &\sum_{m\in[M]} b_m = 1, \quad \boldsymbol{b} \in (\mathbb{R}^+)^M. \end{aligned} \tag{39}$$

where, compared with (35), the indicator function in the objective function is removed due to the minimum SE requirements. Accordingly, $\boldsymbol{\theta}^*$ is obtained as in Section IV-B. For the bandwidth allocation, we also first assign the minimum bandwidth fraction $b_m^0 = R_m/c_m^*$, $m \in [M]$, that satisfies the minimum SE constraint. If $\sum_{m\in[M]} b_m^0 \le 1$ is satisfied, the remaining bandwidth is allocated to the tier

$$m = \mathrm{argmax}_{i\in[M]} \tilde{\lambda}_i c_i^*, \tag{40}$$

which is the same in the ASE optimization case. If not, the revised problem has no solution.

TABLE 1. SYMBOLS AND DESCRIPTION

Symbol	Description	Default value
λ_1, μ_1	The density of β-GPP, and transmit power	$1 \times 10^{-5}, 1$
β	The degree of repulsion of the β-GPP	1
λ_2, μ_2	The density of PPP, and transmit power	$5 \times 10^{-5}, 1$
λ_3, μ_3	The density of MCP, and transmit power	$2.5 \times 10^{-4}, 1$
$\lambda_{\rm p}$	The density of the parent point process for MCP	5×10^{-5}
ϱ	The mean number of points in each cluster for MCP	5
$r_{\rm c}$	The radius of each cluster for MCP	20
α	The path loss exponent	4
G_k	The SIR gain for tier k	N/A
$\tilde{G}_m$	The SIR gain for composite tier m	N/A
R_k	The minimum SE requirement for tier k	0.1
a_k	The power amplifier efficiency of the BSs in tier k	5.5
ϖ_k	The static power consumption of the BSs in tier k	20

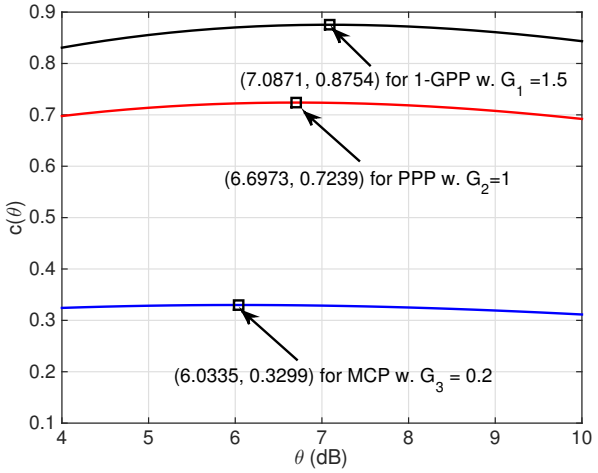

FIGURE 1. The achieved spectral efficiency of the typical user for different tiers with $\alpha = 4$.

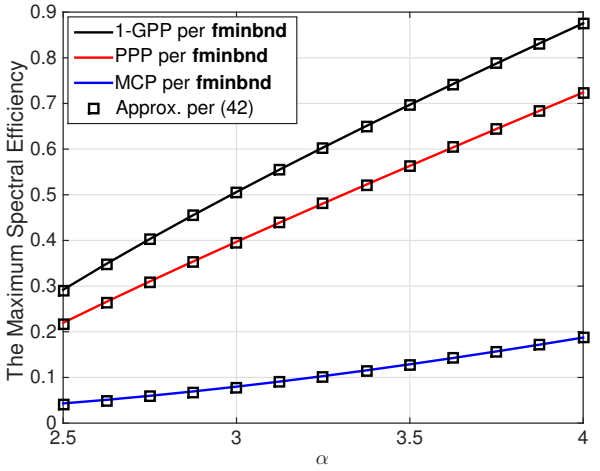

FIGURE 2. The maximum spectral efficiency and its approximation (42) for different α.

For the fairness constraints, Subproblem 2 is revised by replacing the extra constraint based on (39), and thus the optimal spectrum allocation is the same as that for ASE optimization with the fairness constraints.

VI. NUMERICAL RESULTS

In this section, we first present the numerical results of a three-tier general HCN constituted by a β-Ginibre point process (β-GPP) [16], a PPP and a Matérn cluster process (MCP) [28, Chapter 3]. Specifically, the β-GPP models the spatial distribution of the BS tier with repulsion, where β captures the degree of repulsion and λ_1 is the density. The PPP models the spatial distribution of the BS tier with independent behavior and the density is λ_2. The MCP models the spatial distribution of the BS tier with clustering behavior, where the parent point process of the MCP follows a PPP of density $\lambda_{\rm p}$ and for each parent point x, the daughter points of each cluster are uniformly distributed within a ball $B(x, r_{\rm c})$ with a mean number ϱ. The density of the MCP is $\lambda_3 = \lambda_{\rm p}\varrho$. The main symbols and parameters are summarized in Table 1, and default values are given where applicable.

A. OPTIMUM SIR THRESHOLD

Since all the optimization problems considered can be solved in two cascaded steps, first over $\boldsymbol{\theta}$ and then $\boldsymbol{b}$, we first investigate the optimum SIR thresholds for different tiers modeled by different point processes. Fig. 1 shows the spectral efficiency $c(\theta)$ of the typical user for different SIR thresholds and gives the optimum SIR threshold that maximizes the spectral efficiency. It is shown that a larger asymptotic SIR gain yields a better spectral efficiency, which is consistent with the spatial statistics of the different point processes. Namely, point processes with repulsion yield less interference than the ones with attraction (clustering). We also observe that the value of $c(\theta)$ is quite insensitive to θ and the optimum θ are quite close for different G. Therefore, even if the optimum θ is not chosen precisely (say 7 dB), $c(\theta)$ will still be essentially optimum. Hence we provide a simple approximation for the optimum SIR threshold through observing the numerical results, given by

$$\theta^* \approx \hat{\theta} = \frac{7}{2}(\alpha - 2)\ (\text{dB}), \tag{41}$$

TABLE 2. Details of the five EONs for $K = 3$

Spectrum allocation	Composite tier 1		Composite tier 2		Composite tier 3	
	$\tilde{\lambda}_1 =$	$\tilde{G}_1 =$	$\tilde{\lambda}_2 =$	$\tilde{G}_2 =$	$\tilde{\lambda}_3 =$	$\tilde{G}_3 =$
$\mathcal{T}_1=\{1\},\mathcal{T}_2=\{2\},\mathcal{T}_3=\{3\}$	λ_1	G_1	λ_2	G_2	λ_3	G_3
$\mathcal{T}_1=\{1\},\mathcal{T}_2=\{2,3\}$	λ_1	G_1	$\lambda_2+\lambda_3$	$1+\sum_{i\in\{2,3\}}\frac{(\lambda_i\mu_i^{\delta})^2(G_i-1)}{\left(\Sigma_{i\in\{2,3\}}\lambda_i\mu_i^{\delta}\right)^2}$	N/A	N/A
$\mathcal{T}_1=\{1,2\},\mathcal{T}_2=\{3\}$	$\lambda_1+\lambda_2$	$1+\sum_{i\in\{1,2\}}\frac{(\lambda_i\mu_i^{\delta})^2(G_i-1)}{\left(\Sigma_{i\in\{1,2\}}\lambda_i\mu_i^{\delta}\right)^2}$	λ_3	G_3	N/A	N/A
$\mathcal{T}_1=\{1,3\},\mathcal{T}_2=\{2\}$	$\lambda_1+\lambda_3$	$1+\sum_{i\in\{1,3\}}\frac{(\lambda_i\mu_i^{\delta})^2(G_i-1)}{\left(\Sigma_{i\in\{1,3\}}\lambda_i\mu_i^{\delta}\right)^2}$	λ_2	G_2	N/A	N/A
$\mathcal{T}_1=\{1,2,3\}$	$\lambda_1+\lambda_2+\lambda_3$	$1+\sum_{i\in\{1,2,3\}}\frac{(\lambda_i\mu_i^{\delta})^2(G_i-1)}{\left(\Sigma_{i\in\{1,2,3\}}\lambda_i\mu_i^{\delta}\right)^2}$	N/A	N/A	N/A	N/A

and thus an approximation for the maximum spectral efficiency c_m^* is given as

$$c_k^* \approx \frac{\log_2(1+10^{0.35(\alpha-2)})}{{}_2F_1\left(1,-\delta,1-\delta,-10^{0.35(\alpha-2)}/G_k\right)}. \tag{42}$$

Fig. 2 demonstrates the approximation (42) is quite accurate in terms of the optimum spectral efficiency for different α and G, because the value of $c_k(\theta)$ is quite insensitive to θ. Hence, the approximation will greatly accelerate the solution to the problem by obviating the use of the numerical nonlinear optimization tool **fminbnd**.

B. EQUIVALENT ORTHOGONAL NETWORK MODEL

For the tier set $[3]$, all possibilities of the set partitioning is 5 (i.e., the Bell number is 5), and we consider all five different EONs, which correspond to the five types of spectrum allocation schemes. Table 2 shows how to obtain the density and the SIR gain of each composite tier for different EONs via the parameters of the original HCNs.

C. AREA SPECTRAL EFFICIENCY

Here we present the numerical results concerning the ASE in the three-tier HCN.

Fig. 3 shows how different spectrum allocation schemes affect the ASE for different densities of tier 2 and 3 under the case of no SE constraints. It is shown that the ASEs of different spectrum allocation schemes decrease or stay unchanged in the beginning phase of the increasing density ratio. The decline of the ASE is due to the SIR performance degradation caused by the inter-tier interference between the tiers sharing the same spectrum, and the fixed ASE results from the fact that the whole spectrum is allocated to tier 1. We also observe that the spectrum sharing schemes (e.g., $\mathcal{T}_1 = \{1,2,3\}$) are not always the best in terms of the ASE performance. As the density ratio continues to increase, the increasing densities of the tier 2 and 3 compensate the SIR performance degradation and thus result in an ASE improvement.

Fig. 4 shows the impact of the transmit power on the ASE performance. As the transmit power of the BSs in the tier 2 and 3 increases, the ASE stays fixed or decreases

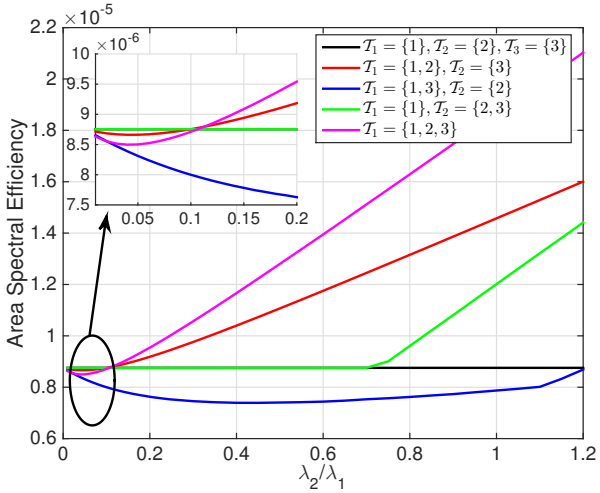

FIGURE 3. The optimal ASE for different spectrum allocation schemes versus the density ratio λ_2/λ_1 with $\lambda_2 = \lambda_3$, $\mu_1 = 1$, $\mu_2 = 25\mu_1$, $\mu_3 = 50\mu_1$, $r_c = 10$, and $\varrho = 10$.

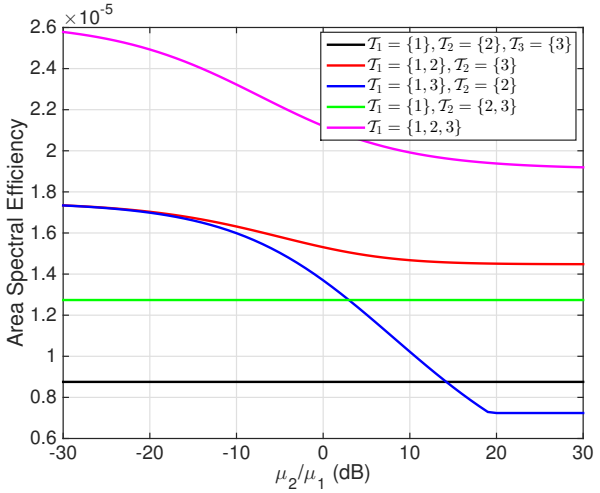

FIGURE 4. The optimal ASE for different spectrum allocation schemes versus the power ratio μ_2/μ_1 with $\lambda_1 = \lambda_2 = \lambda_3 = 1 \times 10^{-5}$, $\mu_1 = 1$, $r_c = 10$, and $\varrho = 10$.

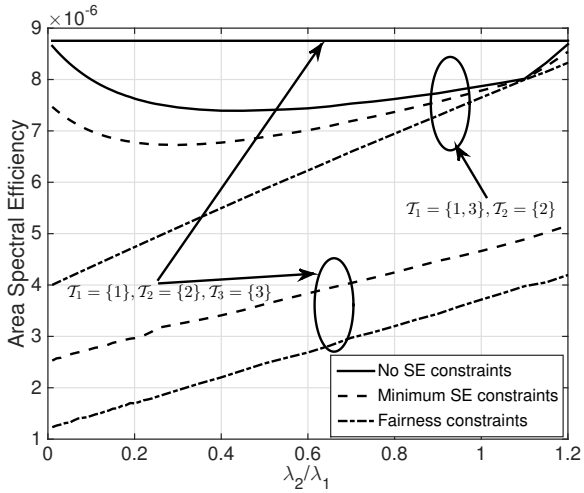

FIGURE 5. The optimal ASE for different constraints versus the density ratio λ_2/λ_1 with $\alpha = 4$, $\lambda_1 = 10^{-5}$, $\lambda_2 = \lambda_3$, $\mu_1 = 1$, $\mu_2 = 25\mu_1$, $\mu_3 = 50\mu_1$, $r_c = 10$, and $\varrho = 10$.

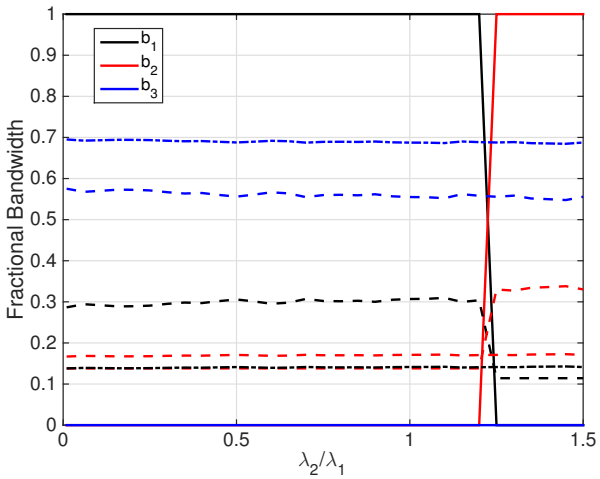

FIGURE 6. The optimal fractional bandwidth $\boldsymbol{b}^*$ for different constraints versus the density ratio λ_2/λ_1 with $\alpha = 4$, $\lambda_1 = 10^{-5}$, $\lambda_2 = \lambda_3$, $\mu_1 = 1$, $\mu_2 = 25\mu_1$, $\mu_3 = 50\mu_1$, $r_c = 10$, and $\varrho = 10$. The solid, dashed and dashed-dot curves are for the cases with no SE constraint, minimum SE constraint and fairness constraint, respectively.

until a certain value is achieved. The reason is the same as that in Fig. 3. The reason why the ASE for the case of $\mathcal{T}_1 = \{1,3\}, \mathcal{T}_2 = \{2\}$ becomes flat at about 19 dB is that the entire bandwidth is first allocated to $\mathcal{T}_1 = \{1,3\}$ and then allocated to $\mathcal{T}_1 = \{2\}$ as the transmit power increases.

Fig. 5 shows how the ASE varies with the density ratios for different spectrum allocation schemes with different constraints. The case with no SE constraints serves as a benchmark, and the performance variation has been illustrated in Fig. 3. In the case with minimum SE constraints, the ASE for the spectrum sharing decreases first and then increases, and the ASE for the spectrum partitioning increases linearly with the density ratio. The reason of the ASE curve trend with increasing density ratio shown in Fig. 5 is the same as in the case with no constraints. In the case of fairness constraints, both ASEs increase linearly with the density ratio. We also observe that the ASE without SE constraints outperforms that with SE constraints. This is because the constraint mandates the allocation of resources to the tiers with lower $\lambda_k c_k^*$ (PPP and MCP tier) to guarantee the corresponding user performance, thus reducing the overall ASE.

Fig. 6 plots the fractional bandwidth $\boldsymbol{b} = (b_1, b_2, b_3)$ as a function of different densities of tier 2 and 3 for the full spectrum partitioning schemes with minimum SE and fairness constraints. It is shown that the case with no SE constraint allocates the entire spectrum to a single tier. We also observe that the fractional bandwidth vector $\boldsymbol{b}$ in the fairness case stays nearly fixed as the density ratio increases, and $\boldsymbol{b}$ in no and minimum SE cases changes suddenly at $\lambda_2/\lambda_1 \approx 1.2$, which is due to $\lambda_2 c_2^* > \lambda_1 c_1^*$ as the density ratio increases.

The above results show that deploying dense BSs with low transmit power is beneficial to improve the ASE for the HCNs for different spectrum allocation schemes and constraints, and different spectrum allocation schemes have their own operating regimes.

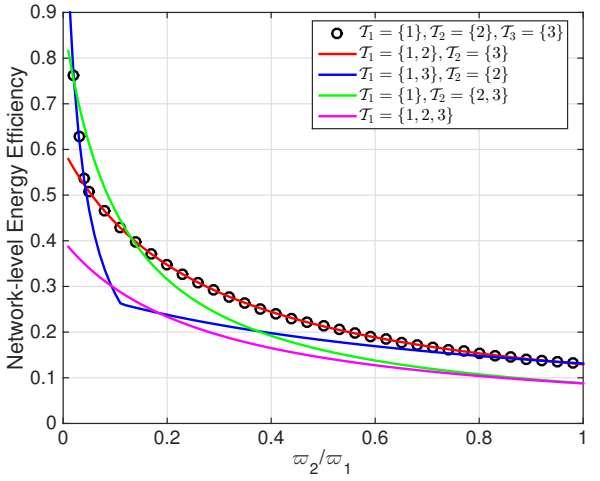

FIGURE 7. The optimal NEE for different spectrum allocation schemes versus ϖ_2/ϖ_1 with $\alpha = 4$, $\mu_1 = 1$, $\mu_2 = \mu_3 = 0.1\mu_1$, and $\varpi_3 = 0.1\varpi_2$.

D. NETWORK ENERGY EFFICIENCY

We present the numerical results concerning the NEE in the three-tier HCN with default densities for different tiers, i.e., a dense deployment for tier 2 and 3.

Fig. 7 shows how different spectrum allocation schemes affect the corresponding NEE with the varied static power consumption of the BSs in tier 2 and 3 under the case of no SE constraints. The spectrum sharing scheme of $\mathcal{T}_1 = \{1,2,3\}$ is not the best in term of NEE, in contrast to the ASE performance. For the spectrum partitioning scheme of $\mathcal{T}_m = \{m\}, m = 1,2,3$, the entire bandwidth is first allocated to tier 2 (the same as $\mathcal{T}_1 = \{1,3\}, \mathcal{T}_2 = \{2\}$) and then to tier 3 (the same as $\mathcal{T}_1 = \{1,2\}, \mathcal{T}_2 = \{3\}$), as the static power consumption increases.

Fig. 8 shows how the NEE varies with the static power

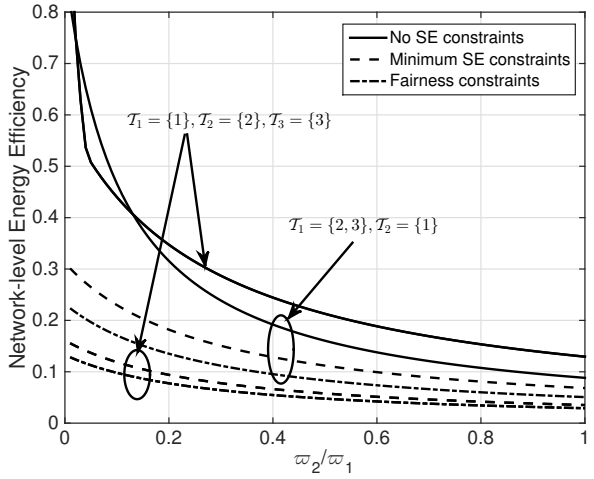

FIGURE 8. The optimal NEE for different constraints versus ϖ_2/ϖ_1 with $\alpha = 4$, $\mu_1 = 1$, $\mu_2 = \mu_3 = 0.1\mu_1$, and $\varpi_3 = 0.1\varpi_2$.

consumption for different spectrum allocation schemes with different constraints. Minimum and fairness constraints lead to worse NEE performance than without SE constraints, because of the high power consumption of tier 1. Since the minimum constraints enable the remaining spectrum resources to improve the ASE performance, it yields better NEE performance than fairness constraints.

The above results show that deploying dense BSs with low power consumption is beneficial to the NEE for the HCNs for different spectrum allocation schemes and constraints.

VII. CONCLUSION

In this paper, a novel framework was proposed to investigate spectrum allocations for general HCNs based on the ASAPPP approximation of SIR distributions. We proposed an equivalent orthogonal network model to capture different configurations of spectrum partitioning and sharing schemes, and further formulated the corresponding optimization problems for both ASE and NEE, which can be solved using the same approach. The optimal solution that maximizes the objective performance metics is to first obtain the optimal SIR thresholds through the ASAPPP method and then give the optimal spectrum allocation based on the optimal SIR thresholds. The insensitivity of the spectral efficiency around the exact optimal SIR threshold yields a simple yet effective approximation to the optimal SIR thresholds and corresponding maximal spectral efficiency. Without a spectral efficiency constraint for each tier, the ASE or NEE is maximized if the entire bandwidth is allocated to a single composite tier, and different spectral efficiency constraints significantly affect the optimal spectrum allocation schemes. The proposed framework provides an efficient approach to find the optimum operating regime for different spectrum allocation schemes for a wide range of network scenarios, which gives key insights to guide the design of HCNs.

REFERENCES

[1] M. Peng, C. Wang, J. Li, H. Xiang, and V. Lau, "Recent advances in underlay heterogeneous networks: Interference control, resource allocation, and self-organization," *IEEE Communications Surveys & Tutorials*, vol. 17, no. 2, pp. 700–729, Second quarter 2015.

[2] Z. Na, Y. Wang, X. Li, J. Xia, X. Liu, M. Xiong, and W. Lu, "Subcarrier allocation based simultaneous wireless information and power transfer algorithm in 5G cooperative OFDM communication systems," *Physical Communication*, vol. 29, pp. 164–170, 2018.

[3] D. Lynch, M. Fenton, D. Fagan, S. Kucera, H. Claussen, and M. O'Neill, "Automated self-optimization in heterogeneous wireless communications networks," *IEEE/ACM Transactions on Networking*, vol. 27, no. 1, pp. 419–432, Feb. 2019.

[4] Y. Zhong, G. Wang, T. Han, M. Wu, and X. Ge, "QoE and cost for wireless networks with mobility under spatio-temporal traffic," *IEEE Access*, vol. 7, pp. 47 206–47 220, 2019.

[5] Y. Chen, B. Ai, Y. Niu, R. He, Z. Zhong, and Z. Han, "Resource allocation for device-to-device communications in multi-cell multi-band heterogeneous cellular networks," *IEEE Transactions on Vehicular Technology*, vol. 68, no. 5, pp. 4760–4773, May 2019.

[6] Z. Na, J. Lv, M. Zhang, B. Peng, M. Xiong, and M. Guan, "GFDM based wireless powered communication for cooperative relay system," *IEEE Access*, vol. 7, pp. 50 971–50 979, 2019.

[7] M. Haenggi, J. Andrews, F. Baccelli, O. Dousse, and M. Franceschetti, "Stochastic geometry and random graphs for the analysis and design of wireless networks," *IEEE Journal on Selected Areas in Communications*, vol. 27, no. 7, pp. 1029–1046, Sep. 2009.

[8] N. Deng and M. Haenggi, "The energy and rate meta distributions in wirelessly powered D2D networks," *IEEE Journal on Selected Areas in Communications*, vol. 37, no. 2, pp. 269–282, Feb. 2019.

[9] H. ElSawy, E. Hossain, and M. Haenggi, "Stochastic geometry for modeling, analysis, and design of multi-tier and cognitive cellular wireless networks: A survey," *IEEE Communications Surveys & Tutorials*, vol. 15, no. 3, pp. 996–1019, Third quarter 2013.

[10] H. ElSawy, A. Sultan-Salem, M. Alouini, and M. Z. Win, "Modeling and analysis of cellular networks using stochastic geometry: A tutorial," *IEEE Communications Surveys & Tutorials*, vol. 19, no. 1, pp. 167–203, First quarter 2017.

[11] W. Bao and B. Liang, "Rate maximization through structured spectrum allocation and user association in heterogeneous cellular networks," *IEEE Transactions on Communications*, vol. 63, no. 11, pp. 4510–4524, Nov. 2015.

[12] N. Deng and M. Haenggi, "SINR and rate meta distributions for HCNs with joint spectrum allocation and offloading," *IEEE Transactions on Communications*, vol. 67, no. 5, pp. 3709–3722, May 2019.

[13] P. D. Mankar, G. Das, and S. S. Pathak, "A novel proportionally fair spectrum allocation in two tiered cellular networks," *IEEE Communications Letters*, vol. 19, no. 4, pp. 629–632, April 2015.

[14] Y. Lin, W. Bao, W. Yu, and B. Liang, "Optimizing user association and spectrum allocation in HetNets: A utility perspective," *IEEE Journal on Selected Areas in Communications*, vol. 33, no. 6, pp. 1025–1039, June 2015.

[15] A. Chattopadhyay, B. Błaszczyszyn, and E. Altman, "Two-tier cellular networks for throughput maximization of static and mobile users," *IEEE Transactions on Wireless Communications*, vol. 18, no. 2, pp. 997–1010, Feb. 2019.

[16] N. Deng, W. Zhou, and M. Haenggi, "The Ginibre point process as a model for wireless networks with repulsion," *IEEE Transactions on Wireless Communications*, vol. 14, no. 1, pp. 107–121, Jan. 2015.

[17] ——, "Heterogeneous cellular network models with dependence," *IEEE Journal on Selected Areas in Communications*, vol. 33, no. 10, pp. 2167–2181, Oct. 2015.

[18] M. Afshang and H. S. Dhillon, "Poisson cluster process based analysis of HetNets with correlated user and base station locations," *IEEE Transactions on Wireless Communications*, vol. 17, no. 4, pp. 2417–2431, April 2018.

[19] M. Haenggi, "ASAPPP: A simple approximative analysis framework for heterogeneous cellular networks," Dec. 2014. Keynote presentation at the 2014 Workshop on Heterogeneous and Small Cell Networks (HetSNets'14) Available at http://www3.nd.edu/~mhaenggi/talks/hetsnets14.pdf.

[20] ——, "The mean interference-to-signal ratio and its key role in cellular and amorphous networks," *IEEE Wireless Communications Letters*, vol. 3, no. 6, pp. 597–600, Dec. 2014.

[21] R. K. Ganti and M. Haenggi, "Asymptotics and approximation of the SIR distribution in general cellular networks," *IEEE Transactions on Wireless Communications*, vol. 15, no. 3, pp. 2130–2143, March 2016.
[22] H. Wei, N. Deng, W. Zhou, and M. Haenggi, "Approximate SIR analysis in general heterogeneous cellular networks," *IEEE Transactions on Communications*, vol. 64, no. 3, pp. 1259–1273, March 2016.
[23] S. S. Kalamkar and M. Haenggi, "Simple approximations of the SIR meta distribution in general cellular networks," *IEEE Transactions on Communications*, vol. 67, no. 6, pp. 4393–4406, June 2019.
[24] M. Haenggi, "The meta distribution of the SIR in Poisson bipolar and cellular networks," *IEEE Transactions on Wireless Communications*, vol. 15, no. 4, pp. 2577–2589, April 2016.
[25] M. Abramowitz and I. A. Stegun, *Handbook of mathematical functions: with formulas, graphs, and mathematical tables*. Courier Corporation, 1964.
[26] Y. Takahashi, Y. Chen, T. Kobayashi, and N. Miyoshi, "Simple and fast PPP-based approximation of SIR distributions in downlink cellular networks," *IEEE Wireless Communications Letters*, vol. 7, no. 6, pp. 898–901, Dec. 2018.
[27] N. Deng, M. Zhao, J. Zhu and W. Zhou, "Traffic-aware relay sleep control for joint macro-relay network energy efficiency," *Journal of Communications and Networks*, vol. 17, no. 1, pp. 47–57, Feb. 2015.
[28] M. Haenggi, *Stochastic geometry for wireless networks*. Cambridge University Press, 2012.

HAICHAO WEI received the B.S. and Ph.D. degrees in information and communication engineering from the University of Science and Technology of China (USTC), Hefei, China, in 2010 and 2016, respectively. Currently he is a lecturer at Dalian Maritime University, Dalian, China. In 2016-2018 he was an Engineer at Huawei Technologies Co., Ltd., Shanghai, China. His research interests include heterogeneous and cellular networks, positioning technologies, stochastic geometry, green communications, and underwater acoustic communications.

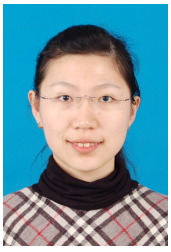

NA DENG (S'12-M'17) received the B.S. and Ph.D. degrees in information and communication engineering from the University of Science and Technology of China (USTC), Hefei, China, in 2010 and 2015, respectively. From 2013 to 2014, she was a Visiting Student with the Prof. Martin Haenggi's group, University of Notre Dame, Notre Dame, IN, USA. From 2015 to 2016, she was a Senior Engineer at Huawei Technologies Co., Ltd., Shanghai, China. She is currently an Associate Professor with the Dalian University of Technology, Dalian, China. Her scientific interests include networking and wireless communications, green communications, and network design based on wireless big data.

MARTIN HAENGGI (S'95-M'99-SM'04-F'14) received the Dipl.-Ing. (M.Sc.) and Dr.sc.techn. (Ph.D.) degrees in electrical engineering from the Swiss Federal Institute of Technology in Zurich (ETH) in 1995 and 1999, respectively. Currently he is the Freimann Professor of Electrical Engineering and a Concurrent Professor of Applied and Computational Mathematics and Statistics at the University of Notre Dame, Indiana, USA. In 2007-2008, he was a visiting professor at the University of California at San Diego, and in 2014-2015 he was an Invited Professor at EPFL, Switzerland. He is a co-author of the monographs "Interference in Large Wireless Network" (NOW Publishers, 2009) and "Stochastic Geometry Analysis of Cellular Networks" (Cambridge University Press, 2018) and the author of the textbook "Stochastic Geometry for Wireless Networks" (Cambridge, 2012), and he published 15 single-author journal articles. His scientific interests lie in networking and wireless communications, with an emphasis on cellular, amorphous, ad hoc (including D2D and M2M), cognitive, and vehicular networks. He served as an Associate Editor of the Elsevier Journal of Ad Hoc Networks, the IEEE Transactions on Mobile Computing (TMC), the ACM Transactions on Sensor Networks, as a Guest Editor for the IEEE Journal on Selected Areas in Communications, the IEEE Transactions on Vehicular Technology, and the EURASIP Journal on Wireless Communications and Networking, as a Steering Committee member of the TMC, and as the Chair of the Executive Editorial Committee of the IEEE Transactions on Wireless Communications (TWC). From 2017 to 2018, he was the Editor-in-Chief of the TWC. He also served as a Distinguished Lecturer for the IEEE Circuits and Systems Society, as a TPC Co-chair of the Communication Theory Symposium of the 2012 IEEE International Conference on Communications (ICC'12), of the 2014 International Conference on Wireless Communications and Signal Processing (WCSP'14), and the 2016 International Symposium on Wireless Personal Multimedia Communications (WPMC'16). For both his M.Sc. and Ph.D. theses, he was awarded the ETH medal. He also received a CAREER award from the U.S. National Science Foundation in 2005 and three awards from the IEEE Communications Society, the 2010 Best Tutorial Paper award, the 2017 Stephen O. Rice Prize paper award, and the 2017 Best Survey paper award, and he is a 2017 and 2018 Clarivate Analytics Highly Cited Researcher.